THE JOURNAL OF PHYSICAL CHEMISTRY C

Article

pubs.acs.org/JPCC

Infrared Spectroscopy and Structures of Boron-Doped Silicon Clusters (Si_nB_m, $n = 3-8$, $m = 1-2$)

Nguyen Xuan Truong,[†,§] Bertram Klaus August Jaeger,[†] Sandy Gewinner,[‡] Wieland Schöllkopf,[‡] André Fielicke,*[,†] and Otto Dopfer*[,†]

[†]Institut für Optik und Atomare Physik, Technische Universität Berlin, Hardenbergstraße 36, D-10623 Berlin, Germany

[‡]Fritz-Haber-Institut der Max-Planck-Gesellschaft, Faradayweg 4-6, D-14195 Berlin, Germany

Supporting Information

ABSTRACT: Binary nanoclusters are of great interest for understanding fundamental phenomena related to applied materials science. Herein, neutral silicon-rich silicon−boron clusters (Si_nB_m, $n = 3-8$, $m = 1-2$) are characterized by means of resonant infrared-ultraviolet two-color ionization (IR-UV2CI) spectroscopy, mass spectrometry, and quantum chemical calculations. Global energy optimizations are employed to find the most stable Si_nB_m structures. By comparing the IR-UV2CI spectrum with the calculated linear IR absorption spectra of the corresponding low-energy isomers, the geometries of the observed Si_nB_m clusters are determined. Based on this structural information, different physical properties of the detected Si_nB_m clusters such as charge distributions and ionization energies are investigated. Natural bond orbital analysis shows that significant negative charge ($\sim -1e$) is localized at the boron atom(s). As the B−B bond is stronger than the B−Si and Si−Si bonds, boron segregation is observed for Si_nB_m clusters with $m = 2$.

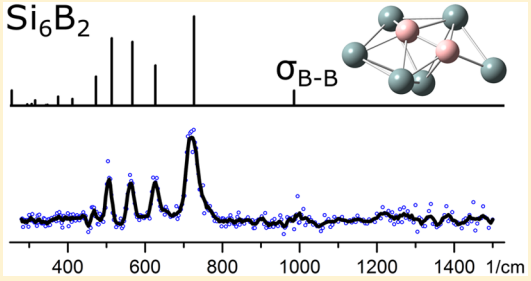

1. INTRODUCTION

Silicon-based nanostructures have attracted particular attention in the current miniaturization trend toward nanophotonics and nanoelectronics.[1−8] In this context, the understanding in the variation of physical and chemical properties as a function of structure, composition, and size at the atomic or molecular level is required. In addition, since the discovery of a superconducting transition in MgB_2 near 40 K,[9] boron has increasingly been used as a source for hole doping in promising superconducting materials, such as boron-doped diamond,[10,11] silicon,[12] and silicon carbide.[13−16] Efforts have been made to increase the critical temperature (T_c) in B-doped silicon, which may benefit from understanding of the bonding of the related atomic clusters at the molecular level.[2,17,18]

So far, studies on boron-doped silicon nanoclusters have however been rare. For example, heats of formation of isolated Si_nB clusters ($n = 1-3$) were measured with Knudsen cell mass spectrometry.[19] Ab initio and density functional theory (DFT) calculations found stable ring-like structures with strong π-bonding interactions for the small SiB_2, Si_2B, and Si_2B_2 clusters.[20,21] Si_nB^- anion clusters ($n = 1-6$) were studied by tandem time-of-flight mass spectrometry and DFT calculations.[22] Therein, Si_6B^- was predicted to have C_{5v} symmetry ($^1A_1$), whereas its neutral counterpart was determined to have a C_s ($^2A'$) geometry.[23] Recently, $Si_6B_2^-$ was concluded to possess a C_1 (^2A) structure from anion photoelectron spectroscopy and calculations.[24] Very recently, the same group reported photoelectron spectra of $B_3Si_n^-$ clusters with $n = 4-10$ and derived cluster structures of the anions by comparison to calculations.[25]

We note that anion photoelectron spectroscopy may not necessarily provide reliable information on the most stable structure of the neutral cluster, in particular for the situation in which the structures in both charge states are quite different. Binding energy considerations for Si_nB cluster growth show that each Si_nB cluster is formed by adding a Si atom to $Si_{n-1}B$, rather than adding B to Si_n.[26] Interestingly, pure boron clusters with sizes of up to 20 atoms show quasi-planar structures,[27] while SiB_7 was predicted to have a 3D structure.[28]

Among available spectroscopic methods for neutral clusters, a widely applicable approach is the combination of resonant IR excitation with near threshold photoionization, i.e., IR-UV two-color ionization (IR-UV2CI). This technique relies on the resonant absorption of one (or several) IR photons prior to absorption of a UV photon to lift the total internal energy of the cluster above the ionization threshold.[29−33] This process leads to emission of a photoelectron, and the created cations are detected with mass spectrometry. By scanning the IR photon energy, the ionization efficiency of the cluster is changed upon resonant IR absorption. Consequently, the detected ion intensity as a function of IR frequency closely reflects the IR absorption spectrum of the respective neutral cluster. Combined with quantum chemical simulations, this technique has been successfully applied to determine the

Received: February 9, 2017
Revised: April 7, 2017
Published: April 11, 2017

DOI: 10.1021/acs.jpcc.7b01290
J. Phys. Chem. C 2017, 121, 9560−9571

structures of a variety of inorganic clusters,[30,34] including silicon-based nanoclusters.[23,29,32,33,35]

Herein, small silicon-rich silicon−boron clusters (Si_nB_m, n = 3−8, m = 1−2) are generated in a dual-target dual-laser ablation source and characterized with IR-UV2CI laser spectroscopy coupled to mass spectrometry and quantum chemical calculations. In contrast to anion photoelectron spectroscopy, IR spectroscopy of cold neutral clusters provides direct and reliable information on the structure of the neutral ground electronic state. For each cluster size, properties of low-energy isomers found with global optimization techniques are determined, including vibrational and electronic spectra, ionization energies, and natural bond orbital (NBO) charge distributions. By comparing the measured IR-UV2CI and calculated IR spectra, the geometric structures of the experimentally observed Si_nB_m clusters are determined. The systemic study extends our recent initial report[23] on Si_6B to different cluster sizes and boron concentration, with the main goal of investigating the impact of the size and composition of Si_nB_m on their geometric and electronic properties. As the B−B bond is stronger than the Si−B and Si−Si bonds, one particular question addresses the possibility of segregation processes for clusters with more than one B atom. While bare Si_n clusters prefer 3D geometries for $n \geq 5$,[36] B_m clusters tend to be planar in the small size regime.[27] Hence, sequential substitution of Si atoms by B raises the interesting question at which composition the 3D → 2D transition occurs for a given size ($n + m$).

2. EXPERIMENTAL AND COMPUTATIONAL METHODS

2.1. Experimental Approach. The experimental setup used for IR-UV2CI spectroscopy of boron-doped silicon clusters, including details of the dual-target dual-laser cluster source, is described elsewhere.[23,37] Briefly, mixed Si_nB_m clusters are produced by laser ablation of a Si rod (natural isotopic abundance) and an isotopically enriched ^{11}B rod (99.5%) within a pulsed flow of helium carrier gas. A solenoid valve provides short helium carrier gas pulses at a backing pressure of about 4 bar. Three-body collisions with carrier gas atoms cool the atomic and molecular species produced in the ablation plasma down and clusters are formed. By tuning the laser fluence on each rod, binary cluster distributions with any desired mixing ratio can be produced.[23] The source is extended with a thermally insulated thermalization channel held at 90 K. The molecular beam is collimated by a skimmer with 2 mm diameter. Before passing through a 1 mm aperture located further downstream and held at ∼200 V to deflect charged clusters, neutral Si_nB_m clusters are irradiated with a counter-propagating IR laser beam from the infrared free electron laser located at the Fritz Haber Institute of the Max Planck Society in Berlin, Germany (FHI FEL).[38,39] Subsequently, they are postionized after a delay of 30 μs with photons from an unfocused F_2 excimer laser (E_{F2} = 7.87 eV) in the extraction zone of a reflectron time-of-flight mass spectrometer. The FHI FEL delivers pulsed IR radiation in the wavelength range from 3.5 to 48 μm, with up to 100 mJ within a macropulse of ∼7 μs duration at about 0.4−1% full-width-at-half-maximum (fwhm) bandwidth. If the frequency of the FEL radiation is resonant with an IR active mode of a specific cluster, it absorbs IR photons followed by rapid intracluster vibrational energy redistribution, and its internal energy increases. The ionization efficiency typically follows an S-curve behavior as a function of excitation energy, with a slope depending on the Franck−Condon factors for ionization.[40] An increase in internal energy of the cluster upon IR absorption enhances the ionization yield. An IR-UV2CI spectrum is then obtained from the relative ionization enhancement normalized by the IR photon flux as a function of the IR laser frequency. Such an IR-UV2CI spectrum closely reflects the linear vibrational absorption spectrum of the neutral cluster. In cases, where the vertical ionization energy (VIE) of the cluster is much lower than E_{F2}, the modulation of the ionization efficiency by resonant IR absorption is small, leading to low signal-to-noise ratios in the IR-UV2CI spectrum. In cluster cases, where the VIE is much larger than E_{F2}, resonant IR absorption will also not be effective in changing the ionization yield.

2.2. Computational Methods. Quantum chemical calculations are performed to aid in the structural assignment and to provide additional insight into electronic properties of the Si_nB_m clusters. The most stable structures are located by a genetic algorithm (GA)[41] coupled to DFT calculations, denoted as GA-DFT. Briefly, the GA-DFT approach begins with an initial population of 32 candidate structures (individuals). These candidate structures are generated by randomly distributing the atoms within a sphere with a radius of 1.0 Å × $N^{1/3}$ with N = $n + m$. The total energy obtained from local optimization at the RI-BP86/def-SVP level (TURBOMOLE V6.3.1[42]) serves as the corresponding fitness value. After each generation, a new population is generated by tournament selection and subsequent modifications through crossover (p_{cross} = 0.6) and mutation (p_{mut} = 0.1) operators.[43] Typically, up to thousand candidate structures are evaluated. The lowest-energy structure determined with GA-DFT then serves as a seed structure for a subsequent basin hopping (BH-DFT) search.[32,44] The BH-DFT algorithm uses a Monte Carlo simulation with thousand Monte Carlo steps at a temperature of 1200 K. New structures are created with the significant structure variant using single-atom moves, followed by all-atom moves at every five steps. In general, the GA-DFT and BH-DFT algorithms agree well in finding the lowest-energy isomers. In a further step, the first 20 nonequivalent low-energy isomers resulting from the GA-DFT and BH-DFT approaches are tightly optimized at the TPSS-D3/cc-pVTZ, B3LYP-D3/cc-pVTZ, and G4 levels of theory (GAUSSIAN 09).[45] At these levels, vibrational spectra, VIE values, and natural bond orbital (NBO) populations are calculated. Relative energies are corrected for zero-point vibrational energies. If not stated otherwise, the optimized parameters are given at the TPSS-D3 level. At this level, no scaling factor is applied for vibrational frequencies.[23,32,35]

3. RESULTS AND DISCUSSION

The most stable Si_nB_m structures with n = 3−8 and m = 1−2 found with the global optimization strategies are shown in Figure 1. The structures of higher-lying isomers are provided in Figures S1 and S2 in the Supporting Information (SI). The notation **n.m.*α*** with **n** = 3−8, **m** = 1−2, and ***α*** = **a**, **b**, **c**, etc., is used for the different low-energy Si_nB_m isomers. Table 1 lists symmetry, electronic state, relative energy (ΔE in kJ/mol), and vertical ionization energy (VIE in eV) of the three lowest-energy Si_nB_m structures. Figures 2−13 compare the measured IR-UV2CI spectra of the various Si_nB_m clusters recorded between 280 and 1500 cm^{-1} with the linear IR absorption spectra of the respective low-energy isomers calculated at the TPSS-D3/cc-pVTZ level. A comparison of all IR-UV2CI spectra is available in Figure S3 in SI. The experimental data points are represented by empty circles, along with five-point adjacent averaging curves. In addition, Figures 2−13 reproduce

DOI: 10.1021/acs.jpcc.7b01290
J. Phys. Chem. C 2017, 121, 9560−9571

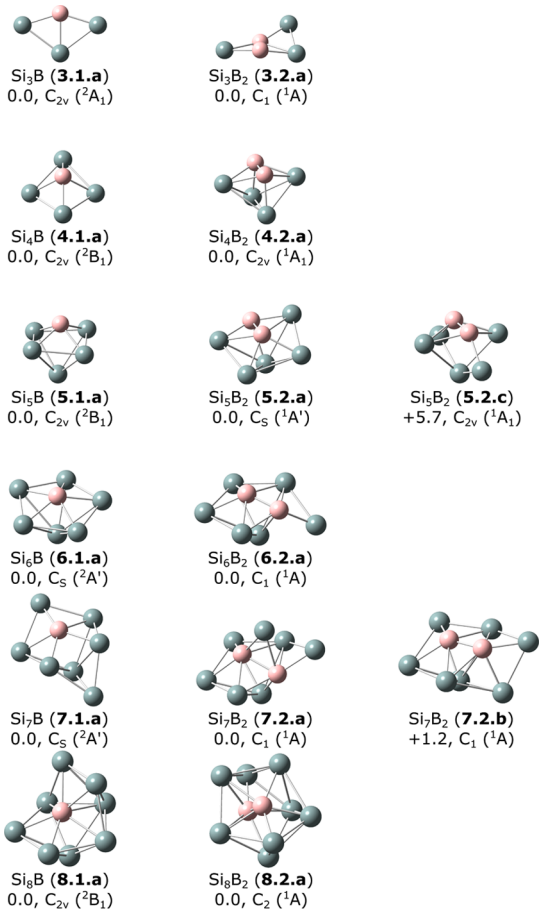

Figure 1. Most stable Si_nB_m structures calculated at the TPSS-D3/cc-pVTZ level (Table 1), along with their relative energy (ΔE in kJ/mol), symmetry, and electronic state. Structures **5.2.c** and **7.2.b** are predicted as global minima at the B3LYP-D3/cc-pVTZ level.

the geometric structures with their symmetry, electronic state, VIE, and ΔE. Cartesian coordinates of all structures are provided in Table S1 in SI. Experimental band positions determined using Gaussian fitting (where applicable) are listed in Table 2 along with their suggested vibrational and isomer assignment. In the following, we separately discuss each individual Si_nB_m cluster size and composition.

3.1. Si_3B. The three most stable structures of Si_3B are found within a relative energy of 35 kJ/mol (Figure 2). Interestingly, they all have a distorted rhomboid-like structure. At the TPSS-D3 level, isomers **3.1.a** and **3.1.b** have a planar C_{2v} ($^2A_1$) geometry, with Si−B−Si angles of β = 145.3° and 78.2°, respectively. Isomer **3.1.c** is similar in energy as **3.1.b** (35 and 33 kJ/mol) and has C_s ($^2A''$) symmetry arising from an out-of-plane B atom. At the B3LYP-D3 level, all three structures are planar, with β = 146.5° (**3.1.a**), 79.0° (**3.1.b**), and 172.6° (**3.1.c**), respectively, but **3.1.b** is a transition state with a vibrational frequency of i774 cm^{-1}. Their VIE values of about 7.8−8.3 eV are well suited for the application of the IR-UV2CI scheme. Our theoretical work supports earlier calculations,[26] which predict structures **3.1.a** and **3.1.b** as the most stable ones. The three considered isomers might be formed through substitution of Si by B in the ground state structure of Si_4 (D_{2h}, ^1A_g).[46,47] For all Si_3B structures, a large geometrical distortion is induced, because the Si−B bond is stronger and shorter than the Si−Si bond. Hence, in the most stable Si_3B isomer, B forms bonds to all three Si atoms. While the three lowest energy structures all have doublet electronic ground states, the two lowest-energy quartet states **3.1.d** and **3.1.e** are very high in energy (130 and 150 kJ/mol).

A close look at the experimental spectrum in Figure 2 reveals three peaks at 686 (A), 739 (B), and 783 cm^{-1} (C). Clearly, none of the individual predicted spectra can explain the

Table 1. Symmetry, Electronic State, Relative Energy (ΔE), and Vertical Ionization Energy (VIE) of the Most Stable Structures of Si_nB_m Calculated at the TPSS-D3/cc-pVTZ, B3LYP-D3/cc-pVTZ, and G4 Levels

		ΔE (kJ/mol)			VIE (eV)	
cluster	sym. (state)	TPSS	B3LYP	G4	TPSS	B3LYP
Si_3B						
3.1.a	C_{2v} ($^2A_1$)	**0.00**	**0.00**	**0.00**	8.16	7.78
3.1.b	C_{2v} ($^2A_1$)	33.3	45.6	29.0	7.83	8.31
3.1.c	C_s ($^2A''$)	35.2	21.7	10.7	8.26	8.27
Si_3B_2						
3.2.a	C_1 (^1A)	**0.0**	**0.0**	**0.0**	7.89	7.99
3.2.b	C_s ($^1A'$)	0.6	21.9	3.2	8.38	8.30
3.2.c	C_2 (^1A)	9.0	11.9	18.2	7.87	7.88
Si_4B						
4.1.a	C_{2v} ($^2B_1$)	**0.0**	**0.0**	**0.0**	7.79	7.55
4.1.b	C_{2v} ($^2A_2$)	32.7	18.2	39.6	7.35	7.13
4.1.c	C_2 (^2B)	33.4	30.3	48.7	7.69	7.55
Si_4B_2						
4.2.a	C_{2v} ($^1A_1$)	**0.0**	**0.0**	**0.0**	7.99	8.03
4.2.b	C_s ($^1A'$)	47.9	27.9	58.7	8.47	8.45
4.2.c	C_s ($^1A'$)	50.1	27.9	63.5	8.09	8.12
Si_5B						
5.1.a	C_{2v} ($^2B_1$)	**0.0**	**0.0**	**0.0**	7.88	7.97
5.1.b	C_s ($^2A'$)	31.2	26.0	39.8	7.82	7.80
5.1.c	C_s ($^2A'$)	48.1	31.4	62.1	7.47	7.43
Si_5B_2						
5.2.a	C_s ($^1A'$)	**0.0**	13.3	3.5	8.08	8.12
5.2.b	C_2 (^1A)	5.2	5.6	12.3	8.04	8.14
5.2.c	C_{2v} ($^1A_1$)	5.7	**0.0**	**0.0**	8.02	8.14
Si_6B						
6.1.a	C_s ($^2A'$)	**0.0**	**0.0**	**0.0**	8.07	8.05
6.1.b	C_{2v} ($^2A_1$)	42.0	48.9	39.9	7.17	7.01
6.1.c	C_2 (^2B)	42.2	29.9	43.6	7.22	7.12
Si_6B_2						
6.2.a	C_1 (^1A)	**0.0**	**0.0**	**0.0**	8.01	8.09
6.2.b	C_s ($^1A'$)	56.1	79.6	56.6	7.78	7.87
6.2.c	C_2 (^1A)	69.9	74.1	85.7	7.39	7.35
Si_7B						
7.1.a	C_s ($^2A'$)	**0.0**	**0.0**	**0.0**	6.98	6.89
7.1.b	C_s ($^2A'$)	8.2	8.0	10.9	6.99	6.84
7.1.c	C_1 (^2A)	10.9	23.0	4.3	7.11	7.09
Si_7B_2						
7.2.a	C_1 (^1A)	**0.0**	3.6	**0.0**	7.87	7.35
7.2.b	C_1 (^1A)	1.2	**0.0**	9.1	7.24	7.21
7.2.c	C_1 (^1A)	24.7	24.8	36.3	7.33	7.30
Si_8B						
8.1.a	C_{2v} ($^2B_1$)	**0.0**	**0.0**	**0.0**	7.34	7.21
8.1.b	C_1 (^2A)	24.1	8.8	34.2	7.18	7.12
8.1.c	C_1 (^2A)	43.0	28.7	56.8	7.32	7.21
Si_8B_2						
8.2.a	C_2 (^1A)	**0.0**	**0.0**	**0.0**	7.51	7.44
8.2.b	C_s ($^1A'$)	7.1	14.8	19.9	7.42	7.73
8.2.c	C_2 (^1A)	12.7	2.4	23.2	7.43	7.47

DOI: 10.1021/acs.jpcc.7b01290
J. Phys. Chem. C 2017, 121, 9560−9571

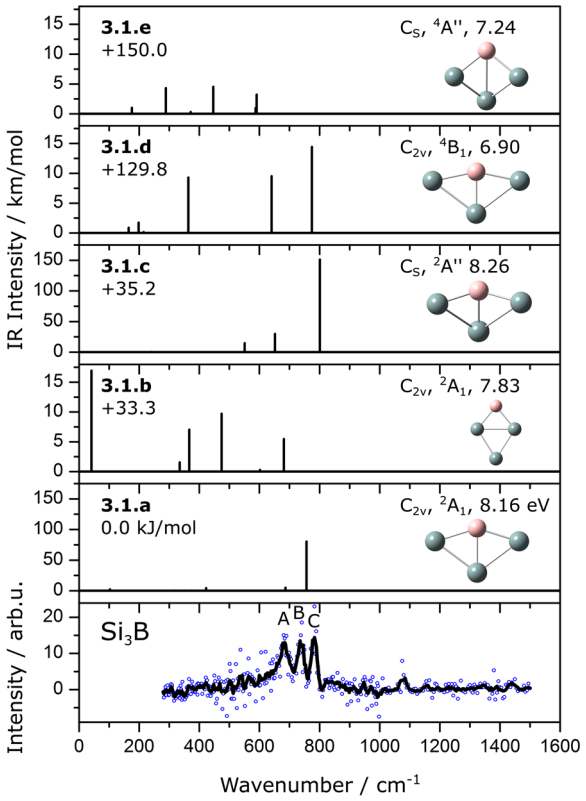

Figure 2. Comparison of IR-UV2CI spectrum of Si_3B with IR absorption spectra calculated for the low-energy structures **3.1.a–e** at the TPSS-D3/cc-pVTZ level (Tables 1 and 2).

experimental one. However, one possibility may be the coexistence of **3.1.a** and **3.1.c**, although the relative intensities in the experimental and predicted spectra differ somewhat. Following this scenario, band *A* is assigned to the Si–B stretch of **3.1.a** at 687 cm^{-1} (a) and **3.1.c** at 651 (a′) cm^{-1}, and bands *B* and *C* are attributed to the antisymmetric Si–B–Si stretch of **3.1.a** at 757 cm^{-1} (b_2) and of **3.1.c** at 801 cm^{-1} (a″), respectively. Although **3.1.b** and **3.1.c** are close in energy, the IR cross sections of the strongest transitions of **3.1.b** are weaker by 1 order of magnitude which may explain why this structure is not detected (if present).

3.2. Si_3B_2. At the TPSS-D3 level, the most stable structure **3.2.a** has a C_1 (^{1}A) geometry with a B–B bond length of 1.663 Å (Figure 3). This B_2 unit is connected to all other Si atoms. This behavior arises from the bond strength order B–B > B–Si > Si–Si and is observed in almost all Si_nB_2 structures found in this work. Structure **3.2.a** can be thought of being produced by adding a Si atom to rhombic Si_2B_2 (C_{2v}, $^1A_1$).[20] At the B3LYP-D3 level, structure **3.2.a** is planar (C_s), while a strongly nonplanar geometry (C_1) is obtained at the TPSS-D3 level. Efforts in calculating a C_s geometry at the TPSS-D3 level lead to a transition state with a low vibrational frequency of *i*91 cm^{-1} and a rather small barrier to planarity of ΔE = +1.2 kJ/mol. The next stable structure **3.2.b** (C_s, ^{1}A′), which is essentially isoenergetic with **3.2.a** (+0.6 kJ/mol), also has a B_2 unit. Structure **3.2.c** (C_2, ^{1}A) is 9 kJ/mol higher in energy, with a nonplanar fan-like shape and the two B atoms lying above and below the Si_3 plane, respectively. In addition, calculations of structure **3.2.c** with the constraint of C_{2v} symmetry result in a low-energy transition state at ΔE = +2.4 kJ/mol and a

Table 2. Comparison of Observed Vibrational Frequencies in the IR-UV2CI Spectra of Si_nB_m (n = 3–8, m = 1–2) with Values Calculated at the TPSS-D3/cc-pVTZ Level

cluster	ν_{exp} (cm^{-1})	ν_{calc} (cm^{-1})[a]	cluster	ν_{exp} (cm^{-1})	ν_{calc} (cm^{-1})[a]
Si_3B	686 (*A*)	687 (a_1, 5, **3.1.a**)	Si_6B_2	464 (*A*)	473 (a, 11, **6.2.a**)
		651 (a′, 30, **3.1.c**)			
	739 (*B*)	757 (b_2, 80, **3.1.a**)		506 (*B*)	514 (a, 25, **6.2.a**)
	783 (*C*)	801 (a″, 151, **3.1.c**)		564 (*C*)	567 (a, 23, **6.2.a**)
Si_3B_2	491 (*A*)	463 (a, 21, **3.2.a**)		627 (*D*)	627 (a, 15, **6.2.a**)
	698 (*B*)	699 (a, 28, **3.2.a**)		724 (*E*)	727 (a, 33, **6.2.a**)
Si_4B	661 (*A*)	638 (a_1, 5, **4.1.a**)		1000 (*F*)	986 (a, 6, **6.2.a**)
	758 (*B*)	741 (b_2, 73, **4.1.a**)	Si_7B	319 (*A*)	313 (a′, 3, **7.1.a**)
		764 (b_1, 26, **4.1.a**)			326 (a″, 2, **7.1.a**)
Si_4B_2	621 (*A*)	637 (b_2, 5, **4.2.a**)		375 (*B*)	377 (a′, 8, **7.1.a**)
	681 (*B*)	658 (b_1, 23, **4.2.a**)			378 (a″, 2, **7.1.a**)
	711 (*C*)	691 (a_1, 17, **4.2.a**)		442 (*C*)	439 (a′, 12, **7.1.a**)
Si_5B	591 (*A*)	597 (a_1, 7, **5.1.a**)		463 (*D*)	466 (a′, 5, **7.1.a**)
		605 (a′, 3, **5.1.b**)		683 (*E*)	676 (a″, 30, **7.1.a**)
	681 (*B*)	674 (b_2, 24, **5.1.a**)		720 (*F*)	717 (a′, 9, **7.1.a**)
	728 (*C*)	747 (b_1, 4, **5.1.a**)	Si_7B_2	442 (*A*)	444 (a, 36, **7.2.a**)
	817 (*D*)	815 (a′, 4, **5.1.b**)		504 (*B*)	495 (a, 9, **7.2.a**)
Si_5B_2	570 (*A*)	571 (a_1, 12, **5.2.c**)		621 (*C*)	612 (a, 34, **7.2.a**)
		592 (a′, 32, **5.2.a**)		691 (*D*)	692 (a, 16, **7.2.a**)
	693 (*B*)	665 (b_2, 40, **5.2.c**)	Si_8B	486 (*A*)	504 (a_1, 16, **8.1.a**)
		709 (b_1, 79, **5.2.c**)			525 (b_2, 23, **8.1.a**)
		651 (a″, 42, **5.2.a**)		666 (*B*)	660 (b_1, 41, **8.1.a**)
Si_6B	423 (*A*)	421 (a′, 9, **6.1.a**)	Si_8B_2	628 (*A*)	637 (b, 21, **8.2.a**)
	535 (*B*)	540 (a′, 29, **6.1.a**)		664 (*B*)	663 (b, 22, **8.2.a**)
	661 (*C*)	649 (a″, 20, **6.1.a**)			672 (a, 31, **8.2.a**)
		663 (a′, 25, **6.1.a**)		750 (*C*)	769 (a, 13, **8.2.a**)

[a]Symmetries, IR intensities (km/mol), and assigned structures are given in parentheses.

DOI: 10.1021/acs.jpcc.7b01290
J. Phys. Chem. C 2017, 121, 9560–9571

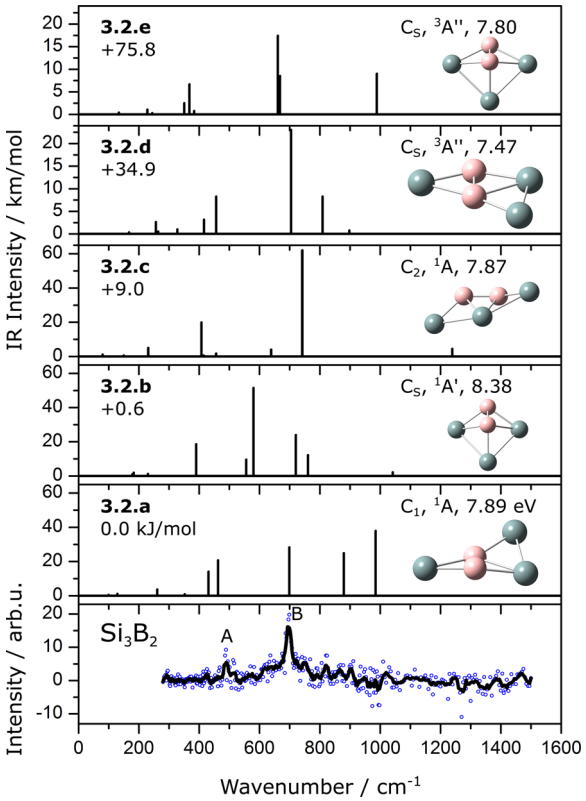

Figure 3. Comparison of IR-UV2CI spectrum of Si_3B_2 with IR absorption spectra calculated for the low-energy structures **3.2.a**–**e** at the TPSS-D3/cc-pVTZ level (Tables 1 and 2).

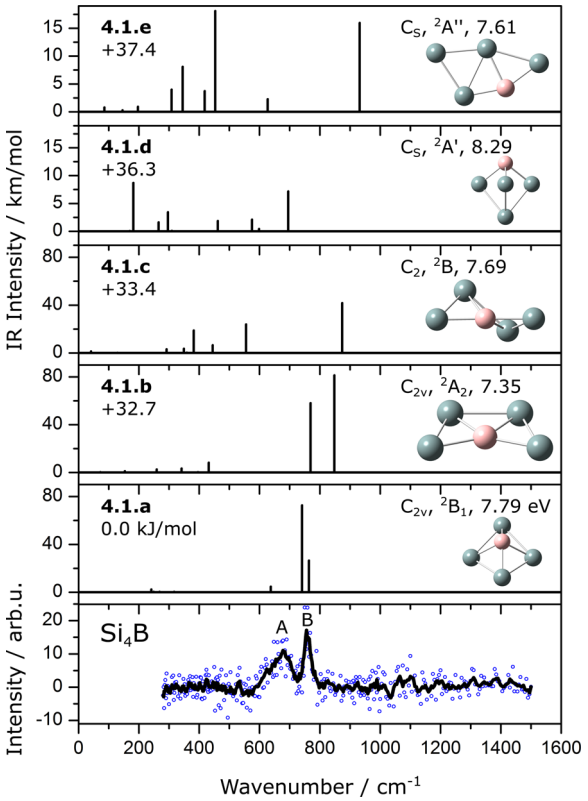

Figure 4. Comparison of IR-UV2CI spectrum of Si_4B with IR absorption spectra calculated for the low-energy structures **4.1.a**–**e** at the TPSS-D3/cc-pVTZ level (Tables 1 and 2).

vibrational frequency of $i172$ cm^{-1}. Structure **3.2.d** is a triplet state (C_s, $^3A''$) lying 35 kJ/mol above the ground state. It has a similar topology as **3.2.a** but a planar geometry. While the three lowest energy structures all have singlet electronic ground states, the two lowest-energy triplet states **3.2.d** and **3.2.e** are relatively high in energy (35 and 76 kJ/mol).

The IR-UV2CI spectrum for Si_3B_2 is compared in Figure 3 to the calculated absorption spectra of the five lowest-energy structures **3.2.a**–**e**. Although the signal-to-noise ratio of the measured spectrum is low, the observed features in the low-frequency part of the spectrum are consistent with the spectrum predicted for the global minimum **3.2.a**. Following this interpretation, the two clear absorption bands peaking at 491 (A) and 698 cm^{-1} (B) are assigned to coupled Si–B and B–B stretch modes predicted at 463 and 699 cm^{-1}, respectively. Apparently, the strong transitions predicted above 800 cm^{-1} are not observed experimentally, and we currently cannot offer any obvious explanation for this discrepancy. At first glance, based on the peak pattern also an assignment to the low-energy isomer **3.2.c** (+9 kJ/mol) may be possible. However, the splitting of the two intense bands predicted at 407 and 741 cm^{-1} (334 cm^{-1}) is much larger than the observed one (207 cm^{-1}) and also the absolute frequency deviation from the experimental band A at 491 cm^{-1} is unusually large. At this stage, a clear-cut assignment to a certain structural isomer is not possible.

3.3. Si_4B. Figure 4 compares the IR-UV2CI spectrum recorded for Si_4B with linear IR absorption spectra computed for the first five low-energy isomers **4.1.a**–**e**. The experimental spectrum reveals two bands peaking at ~661 (A) and 758 cm^{-1} (B). Despite the limited quality of the experimental spectrum, only the spectrum predicted for the doublet ground state **4.1.a** (C_{2v}, $^2B_1$) shows good agreement. Although the predicted isomer **4.1.b** has a similar spectral pattern as the one observed experimentally, the absolute frequencies show an unusally large deviation of around 16.5 and 12% (109 and 90 cm^{-1}), respectively, which cannot readily be accounted for by anharmonicity. Following the assignment to **4.1.a**, band A is assigned to the breathing (i.e., symmetric Si–B stretch) mode at 638 cm^{-1} (a_1), and band B is attributed to the overlap of the antisymmetric Si–B stretch modes at 741 (b_2) and 764 cm^{-1} (b_1). Structure **4.1.a** is a distorted triangular bipyramid, formed by either adding a B atom to the most stable Si_4 structure (D_{2h}, ^1A_g) or by substituting a Si atom with B in the triangular base of the Si_5 bipyramid (D_{3h}, $^1A_1'$). The next four higher energy structures are all located between 30 and 40 kJ/mol. Structure **4.1.b** (C_{2v}, $^2A_2$) has a planar trapezoidal geometry with a central B atom. Structure **4.1.c** (C_2, ^2B) is a distorted form of **4.1.a** and **4.1.b**, obtained by different rotations of the Si–B–Si motif. Isomer **4.1.d** with C_s ($^2A'$) geometry can be formed by B-substitution of a Si atom at the apex of the triangular Si_5 bipyramid (D_{3h}, $^1A_1'$). Finally, **4.1.e** (C_s, $^2A''$) is obtained by adding a Si atom to structure **3.1.b** (C_{2v}). The low signal-to-noise ratio of the IR-UV2CI spectrum might be related to the large deviation of the VIE values of all considered Si_4B isomers from E_{F2} (Figure 4). Similar to Si_3B, B forms bonds to all available Si atoms in the most stable Si_4B isomer.

3.4. Si_4B_2. The ground state structure **4.2.a** in Figure 5 is a distorted bipyramid (C_{2v}, $^1A_1$), formed by either substituting two neighboring Si atoms (Si_2) in Si_6 (D_{4h}, $^1A_{1g}$) with two B atoms or by adding the B–B motif to Si_4 (D_{2h}, ^1A_g).[46,47] The B–B bond length is about 1.610 Å, and thus substantially

DOI: 10.1021/acs.jpcc.7b01290
J. Phys. Chem. C 2017, 121, 9560–9571

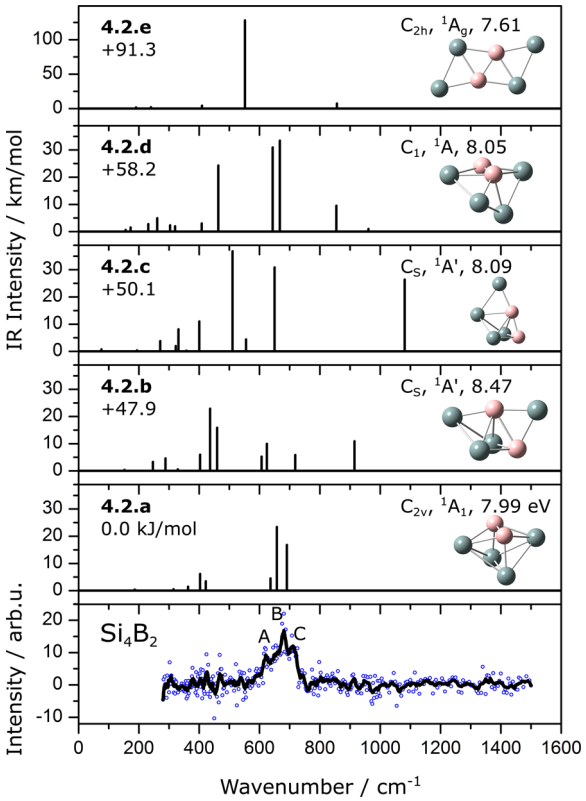

Figure 5. Comparison of IR-UV2CI spectrum of Si_4B_2 with IR absorption spectra calculated for the low-energy structures **4.2.a–e** at the TPSS-D3/cc-pVTZ level (Tables 1 and 2).

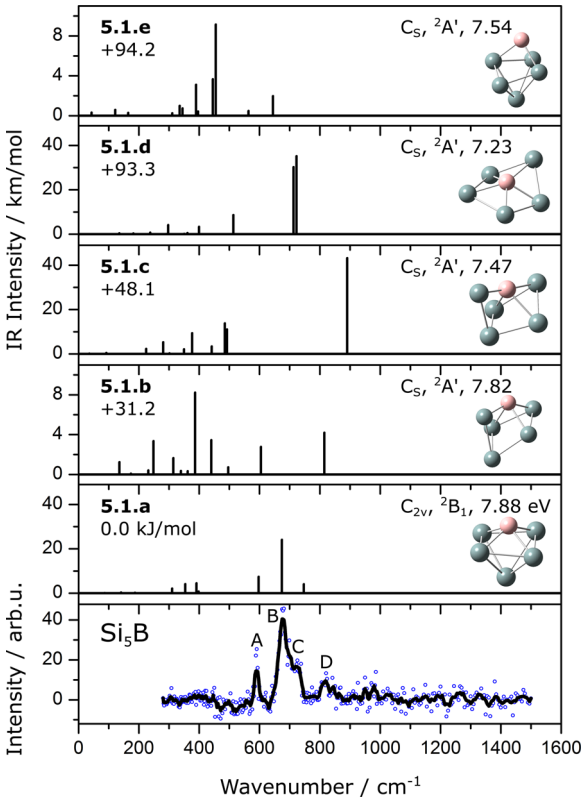

Figure 6. Comparison of IR-UV2CI spectrum of Si_5B with IR absorption spectra calculated for the low-energy structures **5.1.a–e** at the TPSS-D3/cc-pVTZ level (Tables 1 and 2).

shorter than in **3.2.a** (1.663 Å). Its VIE value of 7.99 eV is suitable for the IR-UV2CI scheme. As further structures **4.2.b–e** are at least 47 kJ/mol above the minimum, their contribution to the measured spectrum is not expected. Indeed, the broad observed feature with three peaks at 621 (*A*), 681 (*B*), and 711 cm^{-1} (*C*) can be explained with the three vibrational modes of the ground state structure **4.2.a** predicted with rather low IR intensity at 637 cm^{-1} (antisymmetric Si–B stretch (b_2), 5 km/mol), 658 cm^{-1} (antisymmetric Si–B stretch (b_1), 23 km/mol), and 691 cm^{-1} (symmetric Si–B stretch (a_1), 17 km/mol), respectively.

3.5. Si_5B. Similar to **4.2.a**, the ground state structure **5.1.a** is a strongly distorted tetragonal bipyramid (C_{2v}, $^2B_1$), formed by substituting an apex of the tetragonal bipyramid Si_6 (D_{4h}, $^1A_{1g}$) by B.[47] The next isomer **5.1.b** (C_s, $^2A'$), lying at 31.2 kJ/mol, can be derived by capping a Si_4 rhomb with a Si–B unit. Figure 6 compares the experimental IR-UV2CI spectrum of Si_5B with IR spectra calculated for the first five low-energy isomers **5.1.a–e**. The four absorption bands observed (*A–D*) can mostly be explained with **5.1.a**. Band *A* at 591 cm^{-1} is assigned to the breathing (symmetric Si–B stretch) mode at 597 cm^{-1} (a_1), and bands *B* and *C* at 681 and 728 cm^{-1} are attributed to the antisymmetric Si–B stretch modes at 674 cm^{-1} (b_2) and 747 cm^{-1} (b_1) of **5.1.a**, respectively. Two scenarios are possible for band *D* at 817 cm^{-1}. First, it may arise from an overtone or combination band of **5.1.a**. Second, it may also be explained by the contribution of structure **5.1.b** to the IR-UV2CI spectrum with a predicted antisymmetric Si–B stretch mode at 815 cm^{-1} (a′), although this isomer is calculated to be relatively high in energy (31 kJ/mol). In this case, the in-plane symmetric Si–B stretch mode (a′) of **5.1.b** at 605 cm^{-1} contributes to band *A*.

3.6. Si_5B_2. The five most stable structures **5.2.a–e** are found within a small energy range of about 20 kJ/mol, and the three lowest ones are even within 6 kJ/mol (Figure 6). At the TPSS-D3 level, **5.2.a** is found most stable, whereas at both the B3LYP-D3 and G4 levels, structure **5.2.c** is found lowest in energy. At the latter level, structure **5.2.a** is very close in energy to the global minimum ($\Delta E \approx 4$ kJ/mol), while structure **5.2.b** is 12 kJ/mol above. Both structures **5.2.a** and **5.2.c** can be considered as originating from the pentagonal bipyramid Si_7 (D_{5h}, $^1A_1'$)[32,48] by B-substitution. For **5.2.a**, one Si atom is replaced at an apex and the second in the pentagonal ring. For **5.2.c**, however, two neighboring Si atoms in the ring are substituted by B.

A comparison between the IR absorption spectra calculated for **5.2.a–e** and the IR-UV2CI spectrum measured for Si_5B_2 is provided in Figure 7. The broad features in the experimental spectrum suggest the possible contribution of several isomers. The two peaks identified at 570 (*A*) and 693 cm^{-1} (*B*) can be explained with the coexistence of **5.2.a** (C_s, $^1A'$) and **5.2.c** (C_{2v}, $^1A_1$). At first glance, the overall appearance of the experimental spectrum agrees well with the spectrum calculated for **5.2.c**. Namely, band *A* is assigned to the symmetric Si–B stretch (breathing) mode at 571 cm^{-1} (a_1) and band *B* to the two antisymmetric Si–B stretch modes at 665 (b_2) and 709 cm^{-1} (b_1). In addition, structure **5.2.a** might also contribute to bands *A* and *B* with its symmetric and antisymmetric Si–B stretch modes at 592 (a′) and 651 cm^{-1} (a″), respectively. In addition, the VIE values of about 8 eV predicted for all five considered isomers are favorable for the IR-UV2CI scheme. Although isomer **5.2.b** is also low in energy and has a similar VIE, its presence may be excluded from the absence of its intense

DOI: 10.1021/acs.jpcc.7b01290
J. Phys. Chem. C 2017, 121, 9560–9571

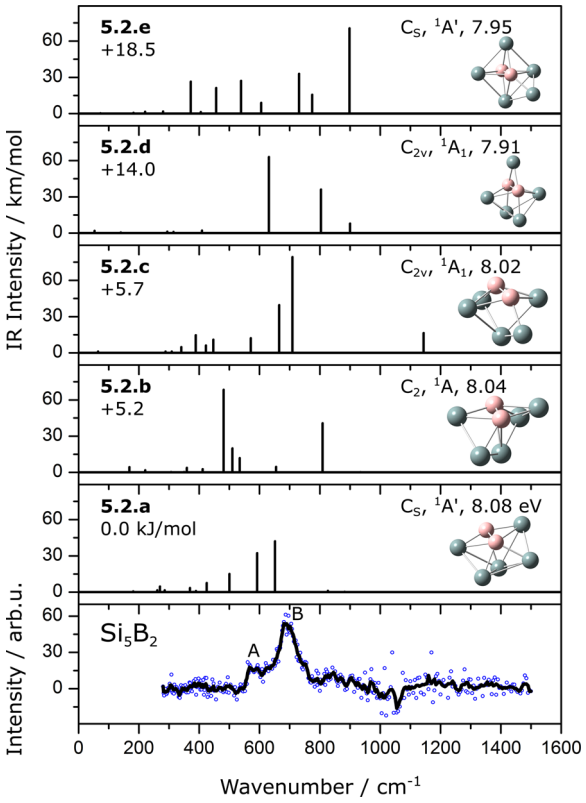

Figure 7. Comparison of IR-UV2CI spectrum of Si_5B_2 with IR absorption spectra calculated for the low-energy structures **5.2.a–e** at the TPSS-D3/cc-pVTZ level (Tables 1 and 2).

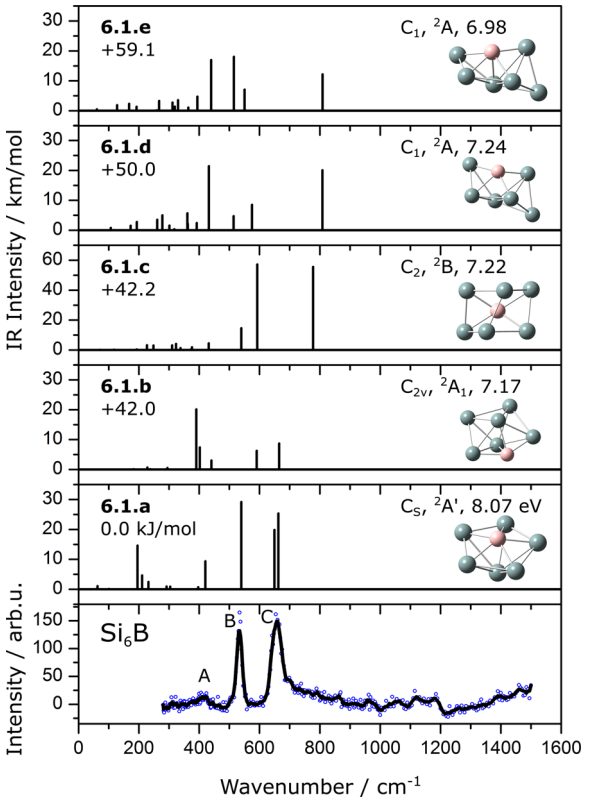

Figure 8. Comparison of IR-UV2CI spectrum of Si_6B with IR absorption spectra calculated for the low-energy structures **6.1.a–e** at the TPSS-D3/cc-pVTZ level (Tables 1 and 2).

predicted high-frequency band at 809 cm^{-1} in the measured spectrum.

3.7. Si_6B. Most results for Si_6B have already been provided in our recent works[23,32] but are included here for completeness (Figure 8). Briefly, the by far most stable structure **6.1.a** is a distorted pentagonal bipyramid (C_s, $^2A'$) formed by substituting a Si atom at an apex of the most stable Si_7 structure (D_{5h}, $^1A_1'$) by B. The VIE value of about 8.0 eV indicates that **6.1.a** should be detected if present in our molecular beam. The next stable structure **6.1.b** with C_{2v} ($^2A_1$) symmetry is about 42.0 kJ/mol higher in energy and formed by B-substitution of a Si atom at the equator of the pentagonal Si_7 bipyramid. These most preferable locations of dopant atoms have been observed previously for, e.g., Si_6C (C_{5v}),[32] Si_6V (C_{2v}), and Si_6Mn (C_{2v}).[49]

The IR-UV2CI spectrum of Si_6B is compared in Figure 8 with the IR absorption spectra of structures **6.1.a–e**. Within the available spectral range, the three experimental bands observed at 423 (*A*), 535 (*B*), and 661 cm^{-1} (*C*) are attributed solely to **6.1.a**. Namely, band *A* is assigned to the equatorial breathing mode at 421 cm^{-1} (a′), band *B* to the axial Si–B stretch mode at 540 cm^{-1} (a′), and band *C* to the overlapping antisymmetric Si–B stretch modes at 649 (a″) and 663 cm^{-1} (a′), respectively.

3.8. Si_6B_2. The ground state of Si_6B_2 (**6.2.a**) has a C_1 (^1A) structure with a VIE value of about 8 eV (Figure 9) and can be obtained by adding a Si atom to **5.2.a**. When compared to the pristine silicon counterpart, **6.2.a** is closer to cationic Si_8^+ (C_{2v}) than to neutral Si_8 (C_{2h}).[29] In Figure 9, the IR-UV2CI spectrum of Si_6B_2 is compared to IR absorption spectra of the first five low-energy isomers **6.2.a–e**. Six experimental bands are observed at 468 (*A*), 506 (*B*), 564 (*C*), 627 (*D*), 724 (*E*), and 1000 cm^{-1} (*F*), which can fully be explained by the **6.2.a**

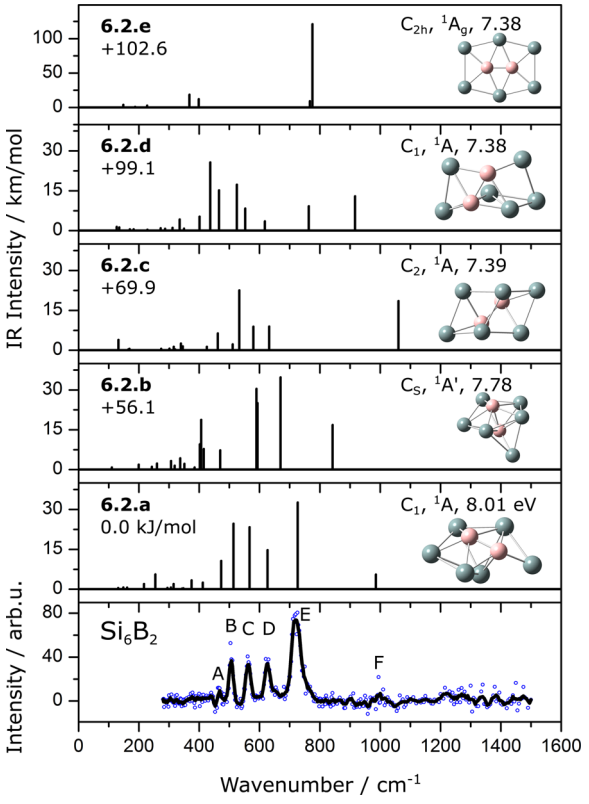

Figure 9. Comparison of IR-UV2CI spectrum of Si_6B_2 with IR absorption spectra calculated for the low-energy structures **6.2.a–e** at the TPSS-D3/cc-pVTZ level (Tables 1 and 2).

DOI: 10.1021/acs.jpcc.7b01290
J. Phys. Chem. C 2017, 121, 9560–9571

global minimum structure. Specifically, bands *A*−*E* are assigned to the symmetric and antisymmetric Si−B stretch modes predicted at 473, 514, 567, 627, and 727 cm^{-1}, respectively, with deviations below 10 cm^{-1}. Interestingly, band *F* is the first observation of the high-frequency B−B stretch vibration predicted at 986 cm^{-1}. Although **6.2.b** has a VIE of 7.78 eV well suited for the IR-UV2CI scheme, none of its intense absorption bands are observed. The structures **6.2.b**−**e** are at least 56 kJ/mol above the global minimum, and thus their contribution to the experimental spectrum of Si_6B_2 can be excluded not only for spectroscopic but also for energetic reasons. The structure **6.2.a**. has also been predicted as global minimum for the neutral and cationic cluster by a recent study combining photoelectron spectroscopy of the $Si_6B_2^-$ anion and computations.[24]

3.9. Si_7B. The ground state structure of Si_7B (**7.1.a**) has C_s ($^2A'$) symmetry and is quite similar to that of **6.2.a** of Si_6B_2. Isomer **7.1.a** might also be formed by adding a Si atom to the ground state of Si_6B (**6.1.a**), or by B-substitution of the bicapped octahedron Si_8 (D_{3d}, $^3A_{2g}$). Note that the calculated VIE value of 6.98 eV for **7.1.a** (and those of all considered higher-energy isomers) is clearly far below the UV photon energy. Figure 10 compares the measured IR-UV2CI spectrum

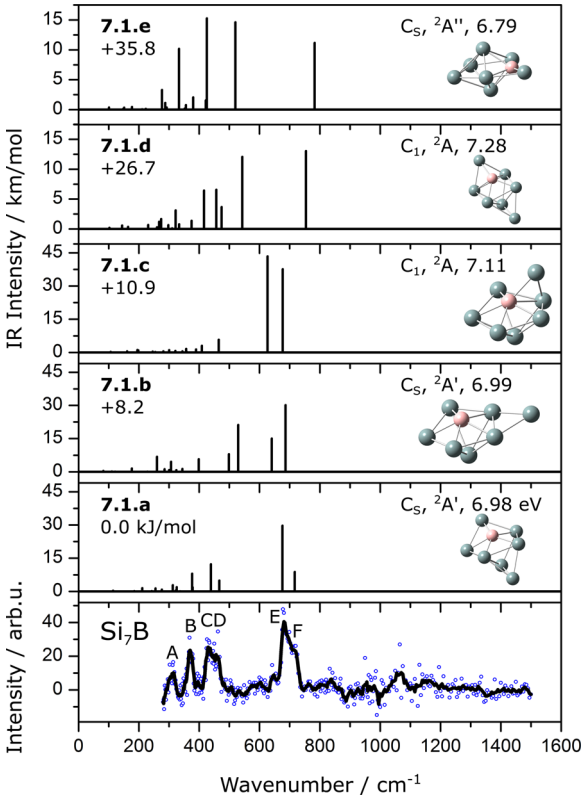

Figure 10. Comparison of IR-UV2CI spectrum of Si_7B with IR absorption spectra calculated for the low-energy structures **7.1.a**−**e** at the TPSS-D3/cc-pVTZ level (Tables 1 and 2).

of Si_7B with IR absorption spectra of the first five low-energy structures **7.1.a**−**e**. Six transitions are observed at 319 (*A*), 375 (*B*), 442 (*C*), 463 (*D*), 683 (*E*), and 720 cm^{-1} (*F*), which all can be explained by the IR spectrum predicted for **7.1.a**. Namely, band *A* is assigned to the a′ mode at 313 cm^{-1} and a″ mode at 326 cm^{-1}. Band *B* is composed of the a′ and a″ modes at 377 and 378 cm^{-1}, respectively. Bands *C*−*F* are assigned to modes calculated at 439 (a′), 466 (a′), 676 (a″), and 717 cm^{-1} (a′), all of which have Si−B stretch character. Apparently, there is no clear spectral signature of any of the higher-energy isomers **7.1.b**−**e** in the measured IR spectrum. Although **7.1.b** and **7.1.c** show similar vibrational pattern as the experimental spectrum, the lack of their strong absorptions predicted at 530 and 627 cm^{-1}, respectively, in the IR-UV2CI spectrum strongly suggests that **7.1.a** is indeed the dominant carrier of the experimental spectrum.

3.10. Si_7B_2. At the TPSS-D3 and G4 levels, the most stable structure of Si_7B_2 is **7.2.a** (C_1, ^1A). The second most stable structure **7.2.b** (C_1, ^1A) is only +1.2 kJ/mol (TPSS-D3) above the minimum. However, at the B3LYP-D3 level, **7.2.b** is predicted as the lowest-energy structure, whereas **7.2.a** is +3.6 kJ/mol higher in energy. These two low-energy structures can be considered as a combination of two common motifs, namely, a deformed pentagonal bipyramid Si_5B_2 (**5.2.a**) and Si_2. The Si_2 motif points closer to the B atom at the apex for **7.2.a**, and to the Si atom at the other apex for **7.2.b**. Figure 11 compares the

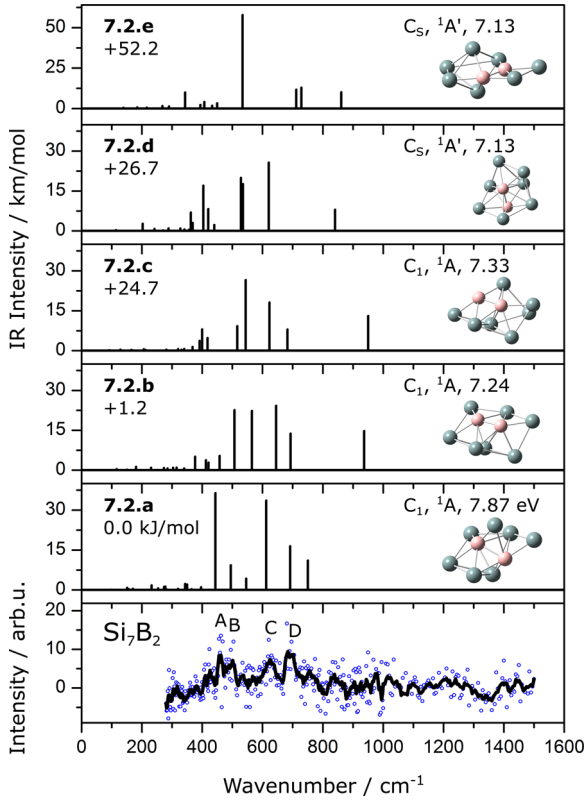

Figure 11. Comparison of IR-UV2CI spectrum of Si_7B_2 with IR absorption spectra calculated for the low-energy structures **7.2.a**−**e** at the TPSS-D3/cc-pVTZ level (Tables 1 and 2).

measured IR-UV2CI spectrum of Si_7B_2 with calculated IR absorption spectra of the five lowest-energy isomers. Despite the low signal-to-noise ratio, four bands can be determined at 442 (*A*), 504 (*B*), 621 (*C*), and 691 cm^{-1} (*D*). At first glance, bands *A*−*D* can be assigned to the vibrational modes of **7.2.a** predicted at 444, 495, 612, and 692 cm^{-1}, respectively. Although some of the transitions of **7.2.b**−**d** are quite close to those of the global minimum, competitive bands at 937 (**7.2.b**), 950 (**7.2.c**), and 840 cm^{-1} (**7.2.d**) are not visible in the experimental spectrum, although at least **7.2.b** is predicted to be very close in energy to the assigned **7.2.a** isomer. Hence,

DOI: 10.1021/acs.jpcc.7b01290
J. Phys. Chem. C 2017, 121, 9560−9571

there is no clear-cut signature of their presence in the experimental spectrum.

3.11. Si_8B. The ground state structure **8.1.a** has C_{2v} ($^2B_1$) symmetry with VIE = 7.34 eV. The next stable structure **8.1.b** (C_1, ^2A) is 24.1 kJ/mol at the TPSS-D3 level (8.8 kJ/mol at the B3LYP-D3 level, 34.2 kJ/mol at the G4 level) higher in energy. On the other hand, **8.1.b** has been predicted as the minimum at the G4 level in recent simulations.[26] Structures **8.1.a** and **8.1.b** are formed by adding Si_2 to **6.1.a**. For **8.1.a**, the Si−Si motif is perpendicular to the Si−B apexes. The measured IR-UV2CI spectrum shows two distinct bands at 486 (*A*) and 666 cm^{-1} (*B*), which can readily be explained by the **8.1.a** global minimum. Structure **8.1.b** may be excluded because its intense transition at 724 cm^{-1} is not observed. All other isomers are very high in energy (>40 kJ/mol).

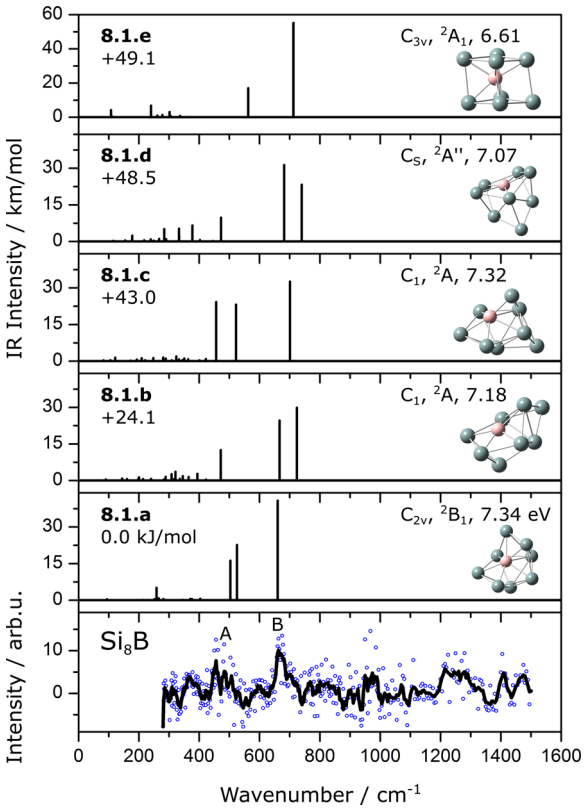

Figure 12. Comparison of IR-UV2CI spectrum of Si_8B with IR absorption spectra calculated for the low-energy structures **8.1.a**−**e** at the TPSS-D3/cc-pVTZ level (Tables 1 and 2).

3.12. Si_8B_2. Structure **8.2.a** (C_2, ^1A) is found as the ground state at all computational levels. In this structure the eight Si atoms are located on a helix around the B−B dimer. Structure **8.2.b** can be thought as formed from Si_{10} (C_{3v}, $^1A_1$) by B-substitution. Similar to **7.2.a** and **7.2.b**, structure **8.2.c** (**8.2.d**) might be generated by adding a Si atom to **7.2.b** (**7.2.a**). The VIEs of all low-energy structures are quite low (7.33−7.51 eV).

The IR-UV2CI spectrum of Si_8B_2 exhibits three clear absorption features at 628 (*A*), 664 (*B*), and 750 cm^{-1} (*C*), which are close to the vibrational modes of structure **8.2.a**, with respect to both frequency and IR intensity. Band *A* is assigned to the Si−B mode at 637 cm^{-1} (b), band *B* corresponds to the overlapping Si−B stretch modes at 663 (b) and 672 cm^{-1} (a), while band *C* arises from the B−B stretch mode at 769 cm^{-1} (a). Closer inspection of the spectra in the low-frequency range

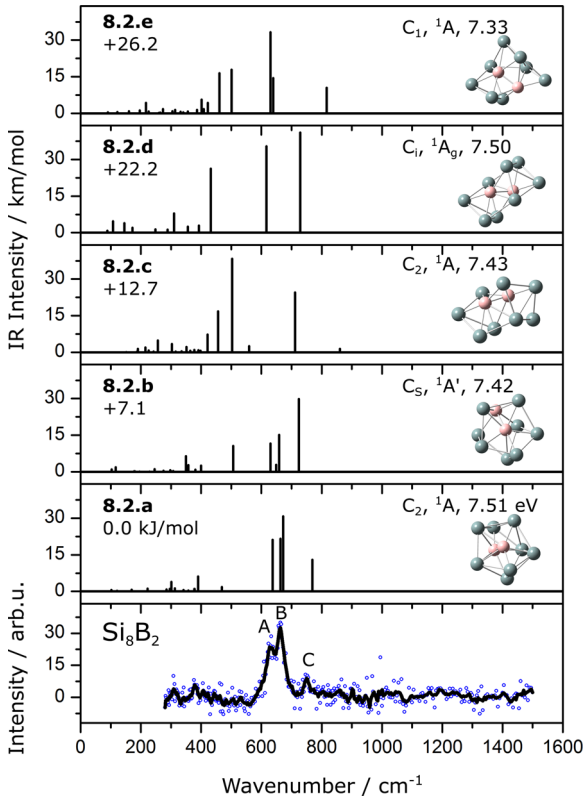

Figure 13. Comparison of IR-UV2CI spectrum of Si_8B_2 with IR absorption spectra calculated for the low-energy structures **8.2.a**−**e** at the TPSS-D3/cc-pVTZ level (Tables 1 and 2).

reveals also good agreement with the Si−Si stretch modes predicted at 301 (b) and 389 cm^{-1} (b) and the weak features measured at 308 and 378 cm^{-1}. Isomer **8.2.b** has strong vibrations calculated at 507 and 724 cm^{-1}, which are not observed experimentally. Similarly, **8.2.c** has intense vibrational modes predicted at 502 and 711 cm^{-1}, which are not observed in the experimental spectrum. Structure **8.2.d** (C_i, ^1A_g) has vibrational modes at 616 cm^{-1} (a_u) and 729 cm^{-1} (a_u) closer to bands *A* and *C*, respectively but the strong mode at 432 cm^{-1} (a_u) is not resolved.

4. FURTHER DISCUSSION

The combined approach of size-selective IR spectroscopy and quantum chemical calculations based on global optimization schemes yields a consistent picture of the cluster growth of B-doped silicon clusters, Si_nB_m, in the size range n = 3−8 and m = 1−2. For most cluster sizes, there is good correspondence between the experimental IR-UV2CI spectra and the linear IR absorption spectra calculated for the most stable structures. To this end, this study provides a first experimental impression of the effects of doping bare silicon clusters with the more electronegative B atoms in neutral mixed Si_nB_m clusters. Comparison with previous computational studies for Si_nB (n = 1−10)[26] and Si_6B_2[24] reveals good agreement with the lowest energy structures for most cluster sizes. Often, the observed spectrum can be explained by the presence of only the predicted most stable structure. Nonetheless, we find substantially more low-energy isomers than previous computations, possibly due to different computational levels and the current application of effective global optimization procedures. For example, the extensive computational study[26] on Si_nB

DOI: 10.1021/acs.jpcc.7b01290
J. Phys. Chem. C 2017, 121, 9560−9571

relevant for the present work completely avoids any global optimization technique.

The B−B bond is significantly stronger than the B−Si and Si−Si bonds. For example, binding energies of the elemental crystals are tabulated as 5.77 and 4.63 eV for B and Si, respectively. Corresponding data for a BSi crystal are not available. In addition, bond lengths and stretching frequencies of the diatomic homodimers B_2 and Si_2 in their $^3\Sigma_g^-$ ground electronic states are listed as r_e = 1.590 and 2.246 Å and ω_e = 1051 and 511 cm^{-1}, respectively,[50] consistent with the smaller atomic size and mass and the stronger chemical bond in B_2. Corresponding experimental data for the BSi heterodimer in its $^4\Sigma^-$ ground state yield intermediate values of r_0 = 1.920 Å and ω_e = 750 cm^{-1}.[51] These data of the crystals and dimer molecules are in line with the parameters observed here for the mixed Si_nB_m clusters. First, the average Si−Si, Si−B, and B−B distances of the most stable Si_nB_m isomers are 2.34−2.56, 1.97−2.21, and 1.66−1.85 Å (Table S2 in SI). They monotonically increase with the cluster size and reflect the order Si−Si > Si−B > B−B expected from the dimer values. Second, the vibrational stretch frequencies appear in the opposite order, Si−Si < Si−B < B−B. Indeed, most of the vibrational modes detected in the IR-UV2CI spectra are Si−B stretch modes occurring in the 400−700 cm^{-1} range. In the Si_nB_2 clusters, the B−B stretch mode has either the highest or second highest frequency, with predicted values of 985, 1005, 827, 986, 692, and 769 cm^{-1} for the most stable **n.2.a** isomers with n = 3−8, respectively. Experimentally, the B−B stretch has only been detected for n = 6 (band F at 1000 cm^{-1}), n = 7 (band D at 691 cm^{-1}), and n = 8 (band C at 746 cm^{-1}), in good agreement with the theoretical predictions. For the other cluster sizes, the IR activity of this mode is below the detection limit. Significantly, all low-energy isomers of Si_nB_2 have a strong B−B bond, i.e., B segregation is observed in Si_nB_m clusters with $m \geq 2$. Similar results have been obtained for $Si_nB_3^-$ anions.[25]

A natural bond orbital analysis performed for the most stable Si_nB_m structures (Table 3, Figure S3 in SI) reveals a high negative charge of around $-e$ located on each of the B atoms. The positive part is then distributed on the Si atoms. This result is similar to the recent analysis of $Si_nB_m^-$ anions[24,25] and confirms that silicon atoms in Si_nB_m clusters are good electron donors, in line with the electronegativity values for these two elements (2.04 for B and 1.90 for Si according to the Pauling scale). There is substantial intraatomic electron transfer from 2s of B to 2p of B, as well as interatomic electron transfer from 3s of Si to 2p of B, which is promoting s-p hybridization of the B atoms.[25]

Table 3. NBO Charges (in e) on B Atom(s) in Selected Si_nB_m Clusters (Figure S3 in the SI)

cluster	isomer	q_B
Si_3B	**3.1.a**	−0.933
Si_3B_2	**3.2.a**	−0.664; −1.049
Si_4B	**4.1.a**	−1.332
Si_4B_2	**4.2.a**	−0.714; −0.714
Si_5B	**5.1.a**	−1.222
Si_5B_2	**5.2.a**	−1.103; −0.835
	5.2.c	−1.052; −1.052
Si_6B	**6.1.a**	−1.407
Si_6B_2	**6.2.a**	−1.107; −1.064
Si_7B	**7.1.a**	−1.531
Si_7B_2	**7.2.a**	−1.464; −1.334
	7.2.b	−1.105; −1.144
Si_8B	**8.1.a**	−1.737
Si_8B_2	**8.2.a**	−1.377; −1.377

5. CONCLUSIONS

Boron−silicon mixed clusters are generated with a dual-target dual-laser ablation source and characterized by means of mass spectrometry, IR-UV2CI spectroscopy, and quantum chemical simulations to provide a first impression of the effects of doping bare neutral silicon clusters with one or two B atoms. The geometric structures of the most stable mixed Si_nB_m clusters (n = 3−8, m = 1−2) are determined by comparison between the calculated and measured IR spectra. For most cluster sizes, there is good correspondence between the measured IR-UV2CI spectra and the IR spectra calculated for the global minimum structures. Due to the low signal-to-noise ratio of some of the IR-UV2CI spectra, some bands are not clear enough to exclude the contribution of other isomers and their coexistence is possible. With the exception of Si_3B and Si_3B_2, convincing agreement is observed between the experimental IR-UV2CI spectrum and the calculated spectra of the isomers lying within 10 kJ/mol of the global minimum. As the B−B bond is stronger than the Si−B and Si−Si bonds, all low-energy Si_nB_2 clusters exhibit a B−B bond. A similar segregation effect has recently been documented for Si_nC_m clusters for doping silicon clusters with carbon.[31] The present study provides for the first time experimental information on Si−B and B−B stretch frequencies in neutral mixed Si_nB_m clusters. These are in accord with the corresponding bond lengths, which vary as Si−Si > Si−B > B−B because of the atomic size, mass, and force constants. Although boron atoms prefer planar cluster structures, up to two B atoms are not sufficient to enforce planar structures in Si_nB_m with $n \geq 3$ and $m \leq 2$. Similarly, although the B atoms tend to maximize the number of bonds to neighboring Si atoms, no endohedral structures are observed up to $n + m$ = 10. In contrast to the high-spin $^4\Sigma^-$ electronic ground state of the SiB dimer,[51,52] the larger Si_nB_m clusters prefer the lowest possible spin state, i.e., singlets for m = even and triplets for m = odd. Interestingly, we show for the first time that the IR-UV2CI technique can be applied to certain Si-containing clusters, which have calculated VIEs well below the postionizing laser photon energy. This might trigger further theoretical efforts to understanding the multiple IR photon absorption mechanism.

■ ASSOCIATED CONTENT

Supporting Information

The Supporting Information is available free of charge on the ACS Publications website at DOI: 10.1021/acs.jpcc.7b01290.

Cartesian coordinates and structures of all isomers; comparison of all experimental IR-UV2CI spectra; NBO charge distribution and average bond distances of most stable isomers. (PDF)

■ AUTHOR INFORMATION

Corresponding Authors

*E-mail: fielicke@physik.tu-berlin.de.

*E-mail: dopfer@physik.tu-berlin.de.

ORCID

Wieland Schöllkopf: 0000-0003-0564-203X

Otto Dopfer: 0000-0002-9834-4404

DOI: 10.1021/acs.jpcc.7b01290
J. Phys. Chem. C 2017, 121, 9560−9571

Present Address

[§]The School of Chemistry, The University of Manchester, Oxford Road, M13 9PL Manchester, United Kingdom.

Notes

The authors declare no competing financial interest.

■ ACKNOWLEDGMENTS

This work was supported by Deutsche Forschungsgemeinschaft within the research unit FOR 1282 (DO 729/5, FI 893/4). N.X.T. thanks the British Nuclear Fuels Ltd. and the Dalton Nuclear Institute for financial support.

■ REFERENCES

(1) Schoning, M. J.; Ronkel, F.; Crott, M.; Thust, M.; Schultze, J. W.; Kordos, P.; Luth, H. Miniaturization of Potentiometric Sensors Using Porous Silicon Microtechnology. *Electrochim. Acta* **1997**, *42*, 3185−3193.

(2) Barnett, R. N.; Landman, U. Cluster-Derived Structures and Conductance Fluctuations in Nanowires. *Nature* **1997**, *387*, 788−791.

(3) Ravindra, N. M. The Drive for Further Miniaturization: Silicon Nanoelectronics. *JOM* **2005**, *57*, 14−15.

(4) Tomioka, K.; Yoshimura, M.; Fukui, T. A III-V Nanowire Channel on Silicon for High-Performance Vertical Transistors. *Nature* **2012**, *488*, 189−192.

(5) Roche, B.; Riwar, R. P.; Voisin, B.; Dupont-Ferrier, E.; Wacquez, R.; Vinet, M.; Sanquer, M.; Splettstoesser, J.; Jehl, X. A Two-Atom Electron Pump. *Nat. Commun.* **2013**, *4*, 1581.

(6) Mirabella, S.; De Salvador, D.; Napolitani, E.; Bruno, E.; Priolo, F. Mechanisms of Boron Diffusion in Silicon and Germanium. *J. Appl. Phys.* **2013**, *113*, 031101.

(7) Huang, K. C. Y.; Seo, M. K.; Sarmiento, T.; Huo, Y. J.; Harris, J. S.; Brongersma, M. L. Electrically Driven Subwavelength Optical Nanocircuits. *Nat. Photonics* **2014**, *8*, 244−249.

(8) Fu, T. M.; Duan, X. J.; Jiang, Z.; Dai, X. C.; Xie, P.; Cheng, Z. G.; Lieber, C. M. Sub-10-nm Intracellular Bioelectronic Probes from Nanowire-Nanotube Heterostructures. *Proc. Natl. Acad. Sci. U. S. A.* **2014**, *111*, 1259−1264.

(9) Nagamatsu, J.; Nakagawa, N.; Muranaka, T.; Zenitani, Y.; Akimitsu, J. Superconductivity at 39 K in Magnesium Diboride. *Nature* **2001**, *410*, 63−64.

(10) Ekimov, E. A.; Sidorov, V. A.; Bauer, E. D.; Mel'nik, N. N.; Curro, N. J.; Thompson, J. D.; Stishov, S. M. Superconductivity in Diamond. *Nature* **2004**, *428*, 542−545.

(11) Yokoya, T.; Nakamura, T.; Matsushita, T.; Muro, T.; Takano, Y.; Nagao, M.; Takenouchi, T.; Kawarada, H.; Oguchi, T. Origin of the Metallic Properties of Heavily Boron-Doped Superconducting Diamond. *Nature* **2005**, *438*, 647−650.

(12) Bustarret, E.; Marcenat, C.; Achatz, P.; Kacmarcik, J.; Levy, F.; Huxley, A.; Ortega, L.; Bourgeois, E.; Blase, X.; Debarre, D.; Boulmer, J. Superconductivity in Doped Cubic Silicon. *Nature* **2006**, *444*, 465−468.

(13) Muranaka, T.; Kikuchi, Y.; Yoshizawa, T.; Shirakawa, N.; Akimitsu, J. Superconductivity in Carrier-Doped Silicon Carbide. *Sci. Technol. Adv. Mater.* **2008**, *9*, 044204.

(14) Kriener, M.; Maeno, Y.; Oguchi, T.; Ren, Z. A.; Kato, J.; Muranaka, T.; Akimitsu, J. Specific Heat and Electronic States of Superconducting Boron-Doped Silicon Carbide. *Phys. Rev. B: Condens. Matter Mater. Phys.* **2008**, *78*, 024517.

(15) Kriener, M.; Muranaka, T.; Kato, J.; Ren, Z. A.; Akimitsu, J.; Maeno, Y. Superconductivity in Heavily Boron-Doped Silicon Carbide. *Sci. Technol. Adv. Mater.* **2008**, *9*, 044205.

(16) Ren, Z. A.; Kato, J.; Muranaka, T.; Akimitsu, J.; Kriener, M.; Maeno, Y. Superconductivity in Boron-Doped SiC. *J. Phys. Soc. Jpn.* **2007**, *76*, 103710.

(17) de Heer, W. The Physics of Simple Metal Clusters: Experimental Aspects and Simple Models. *Rev. Mod. Phys.* **1993**, *65*, 611−676.

(18) Martin, T. P. *Large Clusters of Atoms and Molecules*; Kluwer: Dordrecht, 1996.

(19) Viswanathan, R.; Schmude, R. W.; Gingerich, K. A. Thermochemistry of BSi(g), BSi_2(g), and BSi_3(g). *J. Phys. Chem.* **1996**, *100*, 10784−10786.

(20) Davy, R.; Skoumbourdis, E.; Dinsmore, D. Structure, Energies, Vibrational Spectra and Reactions of the Boron-Silicon Cluster Molecules B_2Si, BSi_2 and B_2Si_2. *Mol. Phys.* **2005**, *103*, 611−619.

(21) Ueno, L. T.; Kiohara, V. O.; Ferrao, L. F. A.; Pelegrini, M.; Roberto-Neto, O.; Machado, F. B. C. Comparative Study of Small Boron, Silicon and Germanium Clusters: B_mSi_n and B_mGe_n (m+n = 2−4). *J. Mol. Model.* **2015**, *21*, 141.

(22) Sun, Z.; Yang, Z.; Gao, Z.; Tang, Z. C. Experimental and Theoretical Investigation on Binary Semiconductor Clusters of B/Si and Al/Si. *Rapid Commun. Mass Spectrom.* **2007**, *21*, 792−798.

(23) Truong, N. X.; Haertelt, M.; Jaeger, B. K. A.; Gewinner, S.; Schöllkopf, W.; Fielicke, A.; Dopfer, O. Characterization of Neutral Boron-Silicon Clusters Using Infrared Spectroscopy: The Case of Si_6B. *Int. J. Mass Spectrom.* **2016**, *395*, 1−6.

(24) Cao, G.-J.; Lu, S.-J.; Xu, H.-G.; Xu, X.-L.; Zheng, W.-J. Structures and Electronic Properties of $B_2Si_6^{-/0/+}$: Anion Photoelectron Spectroscopy and Theoretical Calculations. *RSC Adv.* **2016**, *6*, 62165−62171.

(25) Wu, X.; Lu, S.-J.; Liang, X.; Huang, X.; Qin, Y.; Chen, M.; Zhao, J.; Xu, H.-G.; King, R. B.; Zheng, W. Structures and Electronic Properties of B_3Si_n- (n = 4−10) Clusters: A Combined Ab Initio and Experimental Study. *J. Chem. Phys.* **2017**, *146*, 044306.

(26) Tam, N. M.; Tai, T. B.; Nguyen, M. T. Thermochemical Parameters and Growth Mechanism of the Boron-Doped Silicon Clusters, Si_nB^q with n = 1−10 and q = − 1, 0, + 1. *J. Phys. Chem. C* **2012**, *116*, 20086−20098.

(27) Wang, L.-S. Photoelectron Spectroscopy of Size-Selected Boron Clusters: From Planar Structures to Borophenes and Borospherenes. *Int. Rev. Phys. Chem.* **2016**, *35*, 69−142.

(28) Tai, T. B.; Kadlubanski, P.; Roszak, S.; Majumdar, D.; Leszczynski, J.; Nguyen, M. T. Electronic Structures and Thermochemical Properties of the Small Silicon-Doped Boron Clusters B_nSi (n = 1−7) and Their Anions. *ChemPhysChem* **2011**, *12*, 2948−2958.

(29) Haertelt, M.; Lyon, J. T.; Claes, P.; de Haeck, J.; Lievens, P.; Fielicke, A. Gas-Phase Structures of Neutral Silicon Clusters. *J. Chem. Phys.* **2012**, *136*, 064301.

(30) Haertelt, M.; Fielicke, A.; Meijer, G.; Kwapien, K.; Sierka, M.; Sauer, J. Structure Determination of Neutral MgO Clusters-Hexagonal Nanotubes and Cages. *Phys. Chem. Chem. Phys.* **2012**, *14*, 2849−2856.

(31) Savoca, M.; Lagutschenkov, A.; Langer, J.; Harding, D. J.; Fielicke, A.; Dopfer, O. Vibrational Spectra and Structures of Neutral Si_mC_n Clusters (m + n = 6): Sequential Doping of Silicon Clusters with Carbon Atoms. *J. Phys. Chem. A* **2013**, *117*, 1158−1163.

(32) Truong, N. X.; Savoca, M.; Harding, D. J.; Fielicke, A.; Dopfer, O. Vibrational Spectra and Structures of Neutral Si_6X Clusters (X = Be, B, C, N, O). *Phys. Chem. Chem. Phys.* **2014**, *16*, 22364−22372.

(33) Li, Y. J.; Tam, N. M.; Claes, P.; Woodham, A. P.; Lyon, J. T.; Ngan, V. T.; Nguyen, M. T.; Lievens, P.; Fielicke, A.; Janssens, E. Structure Assignment, Electronic Properties, and Magnetism Quenching of Endohedrally Doped Neutral Silicon Clusters, Si_nCo (n = 10−12). *J. Phys. Chem. A* **2014**, *118*, 8198−8203.

(34) Jalink, J.; Bakker, J. M.; Rasing, T.; Kirilyuk, A. Channeling Vibrational Energy to Probe the Electronic Density of States in Metal Clusters. *J. Phys. Chem. Lett.* **2015**, *6*, 750−754.

(35) Truong, N. X.; Savoca, M.; Harding, D. J.; Fielicke, A.; Dopfer, O. Vibrational Spectra and Structures of Si_nC Clusters (n = 3−8). *Phys. Chem. Chem. Phys.* **2015**, *17*, 18961−18970.

(36) Kostko, O.; Leone, S. R.; Duncan, M. A.; Ahmed, M. Determination of Ionization Energies of Small Silicon Clusters with Vacuum Ultraviolet Radiation. *J. Phys. Chem. A* **2010**, *114*, 3176−3181.

(37) Fielicke, A.; von Helden, G.; Meijer, G. Far-Infrared Spectroscopy of Isolated Transition Metal Clusters. *Eur. Phys. J. D* **2005**, *34*, 83−88.

DOI: 10.1021/acs.jpcc.7b01290
J. Phys. Chem. C 2017, 121, 9560−9571

(38) Schöllkopf, W.; Gewinner, S.; Junkes, H.; Paarmann, A.; von Helden, G.; Bluem, H.; Todd, A. M. M. The New IR and THz FEL Facility at the Fritz Haber Institute in Berlin. *Proc. SPIE* **2015**, *9512*, 95121L.
(39) Schöllkopf, W.; Gewinner, S.; Erlebach, W.; Junkes, H.; Liedke, A.; Meijer, G.; Paarmann, A.; von Helden, G.; Bluem, H.; Dowell, D.; et al. The New IR FEL Facility at the Fritz-Haber-Institut in Berlin. *Proc. of the 36th Free Electron Laser Conference, Basel, Switzerland* **2014**, 629−634.
(40) Sudbo, A. S.; Schulz, P. A.; Krajnovich, D. J.; Lee, Y. T.; Shen, Y. R. Photo-Ionization Study of Multiphoton-Excited SF_6 in a Molecular-Beam. *Opt. Lett.* **1979**, *4*, 219−221.
(41) Wall, M. GAlib: A C++ Genetic Algorithm Library. Available from: http://lancet.mit.edu/ga.
(42) Ahlrichs, R.; Bär, M.; Häser, M.; Horn, H.; Kölmel, C. Electronic-Structure Calculations on Workstation Computers - the Program System Turbomole. *Chem. Phys. Lett.* **1989**, *162*, 165−169. TURBOMOLE V6.3 2011, a development of University of Karlsruhe and Forschungszentrum Karlsruhe GmbH, 1989−2007, TURBOMOLE GmbH, since 2007. Available from: http://www.turbomole.com.
(43) Goldberg, D. E. *Genetic Algorithms in Search, Optimization, and Machine Learning*; Addison-Wesley: Reading, MA, 1989.
(44) Harding, D. J.; Kerpal, C.; Meijer, G.; Fielicke, A. Unusual Bonding in Platinum Carbido Clusters. *J. Phys. Chem. Lett.* **2013**, *4*, 892−896.
(45) Frisch, M. J.; et al. *Gaussian 09*, Revision D.01; Gaussian Inc.: Wallingford, CT, 2009.
(46) Raghavachari, K.; Logovinsky, V. Structure and Bonding in Small Silicon Clusters. *Phys. Rev. Lett.* **1985**, *55*, 2853−2856.
(47) Raghavachari, K. Theoretical-Study of Small Silicon Clusters - Equilibrium Geometries and Electronic Structures of Si_{2-7}, Si_{10}. *J. Chem. Phys.* **1986**, *84*, 5672−5686.
(48) Fielicke, A.; Lyon, J. T.; Haertelt, M.; Meijer, G.; Claes, P.; de Haeck, J.; Lievens, P. Vibrational Spectroscopy of Neutral Silicon Clusters Via Far-IR-VUV Two Color Ionization. *J. Chem. Phys.* **2009**, *131*, 171105.
(49) Claes, P.; Ngan, V. T.; Haertelt, M.; Lyon, J. T.; Fielicke, A.; Nguyen, M. T.; Lievens, P.; Janssens, E. The Structures of Neutral Transition Metal Doped Silicon Clusters, Si_nX (n = 6−9; X = V, Mn). *J. Chem. Phys.* **2013**, *138*, 194301.
(50) Linstrom, P. J.; Mallard, W. G. *Nist Chemistry Webbook*; NIST Standards and Technology: Gaithersburg, MD, http://webbook.nist.gov, (retrieved March 13, 2017).
(51) Brazier, C. R.; Ruiz, J. I.; Parks, S. V. The Electronic Emission Spectrum of SiB. *J. Mol. Spectrosc.* **2007**, *241*, 1−6.
(52) Knight, L. B., Jr.; McKinley, A. J.; Babb, R. M.; Morse, M. D.; Arrington, C. A. Laser Vaporization Generation of the SiB and SiAl Radicals for Matrix Isolation Electron Spin Resonance Studies; Comparison with Theoretical Calculations and Assignment of Their Electronic Ground States as $X\ ^4\Sigma$. *J. Chem. Phys.* **1993**, *98*, 6749−6757.

DOI: 10.1021/acs.jpcc.7b01290
J. Phys. Chem. C 2017, 121, 9560−9571